Transabdominal near infrared oximetry of hypoxic stress in fetal sheep brain *in utero*

Regine Choe*†, Turgut Durduran*, Guoqiang Yu*, Mark J. M. Nijland‡, Britton Chance§, Arjun G. Yodh*, and Nirmala Ramanujam¶

Departments of *Physics and Astronomy and §Biochemistry and Biophysics, University of Pennsylvania, Philadelphia, PA 19104; ‡Laboratory for Pregnancy and Newborn Research, College of Veterinary Medicine, Cornell University, Ithaca, NY 14853-6401; and ¶Department of Biomedical Engineering, University of Wisconsin, Madison, WI 53706

Contributed by Britton Chance, August 25, 2003

The feasibility of transabdominal near-infrared (NIR) spectroscopy for detecting and quantifying fetal hypoxia *in utero* is demonstrated in a pregnant ewe model. A frequency domain NIR spectroscopy probe, consisting of two detectors and six sources operating at three wavelengths (675, 786, and 830 nm), was placed on the maternal abdomen directly above the fetal head. Fetal hypoxia was indirectly induced through occlusion of uterine blood flow for ≈3 min. NIR photon diffusion measurements were made during a baseline period, during hypoxia of the fetus, and during recovery. Fetal blood samples were drawn from the fetal brachial artery and jugular veins at several time points during the cycle. Seven hypoxic cycles were induced in a total of five pregnant ewes. The NIR measurements were analyzed by using a two-layer diffusion model to deconvolve the fetal blood saturation from that of the pregnant ewe. Fetal hypoxia was detected. Good agreement was found between fetal blood saturation determined by the transabdominal NIR method and arterial and venous fetal blood saturation quantified from fetal blood samples by using a hemoximeter.

Hypoxic-ischemic damage to the fetal brain can result in permanent neurodevelopmental impairment or death (1–3). Early detection of fetal cerebral hypoxic ischemia is thus important for timely intervention. Current noninvasive antepartum screening and diagnostic tools for fetal well-being *in utero* include the nonstress test (fetal heart rate monitoring) and the biophysical profile (fetal heart rate monitoring and ultrasound). Fetal heart rate monitoring, however, probes fetal cerebral hemodynamics and oxygenation indirectly and has a high false-positive rate (4, 5). This result has led to an increased number of unnecessary Cesarean sections and premature deliveries (6). Clearly, the development of devices to directly monitor fetal cerebral oxygenation and hemodynamics could improve the specificity of antepartum tests. Near-infrared (NIR) diffuse optical spectroscopy has the potential to noninvasively monitor fetal cerebral oxygenation and hemodynamics *in utero*. NIR light is non-ionizing and the power levels used are harmless to the body, making this technology safe under continuous exposure. Additionally, NIR technology can be designed to be fast and portable and is therefore suitable in a clinical setting.

In the NIR spectral region (650–900 nm), the primary absorbers in brain are oxy- and deoxy-hemoglobin, and, because tissue scattering is much greater than tissue absorption, light is able to penetrate millimeters to centimeters into the tissue before it is collected by the detector. Typically, absorption and scattering coefficients of tissue are quantitatively determined from NIR photon reflectance measurements by using a light transport model based on the diffusion approximation (7). Tissue blood oxygenation and concentration are then easily derived from the absorption coefficients (8–10). Thus far, NIR diffuse optical spectroscopy has been widely applied to functional studies of blood oxygenation and concentration in the brain, breast, and skeletal muscle (11). A few researchers have developed and used NIR oximeters to monitor neonatal cerebral oxygenation (12–16). More recently, a transvaginal NIR fetal oximeter (17, 18) has been developed but can be used only during labor after the amniotic membrane has ruptured.

Development of a noninvasive transabdominal NIR fetal oximeter is challenging but, if successful, could provide a direct assessment of fetal cerebral oxygenation and hemodynamics before labor and delivery. The feasibility of transabdominal NIR continuous wave (CW) spectroscopy was first explored by Ramanujam *et al.* (19, 20) during a non-stress test. Subsequently, Zourabian *et al.* (21) developed a transabdominal NIR CW oximeter with the capability to detect fetal arterial pulses *in utero*. In addition, theoretical and experimental tissue phantom investigations have been performed to understand NIR photon diffusion through the fetal brain *in utero* (22, 23). Collectively, these studies suggest that transabdominal NIR photon diffusion measurements through the fetal brain *in utero* are possible. However, due to limitations of the instrumentation and analytical models used in these studies, it has not as yet been possible to quantify fetal cerebral blood saturation or blood volume *in utero*.

The goal of this study was to demonstrate the feasibility of transabdominal NIR spectroscopy (NIRS) for detecting and quantifying fetal hypoxia *in utero* in a pregnant ewe model (n = 5). We have built a multi-wavelength NIR frequency-domain instrument with the capability to perform NIR photon diffusion measurements through tissue over a wide range of source-detector separations. We also developed a two-layer numerical diffusion model (for the maternal and fetal layers) to quantify fetal cerebral blood saturation *in utero*. Good agreement was found between fetal blood saturation determined by the transabdominal NIR method, and arterial and venous fetal blood saturation was quantified from fetal blood samples by using a hemoximeter (gold standard). We conclude that transabdominal NIR oximetry has the capability to quantify different degrees of hypoxia in the fetal brain *in utero*.

Materials and Methods

Instrumentation. We designed a multi-wavelength, multi-separation NIR frequency-domain instrument and probe for transabdominal NIR spectroscopy. Fig. 1 shows a schematic of the transabdominal probe and the NIR frequency-domain instrument to which the probe is coupled. The probe was designed as a linear array consisting of two detector fibers and six source fibers. This probe is capable of performing NIR photon diffusion measurements at a total of 12 source-detector separations ranging from 1.8 to 9.5 cm. However, in this study, NIR photon diffusion measurements at 8 source-detector separations ranging from 1.8 to 4 cm (Fig. 1*a*) were sufficient for retrieval of fetal cerebral blood saturation. The instrument consists of a light source module and two detection modules. It is described in

Abbreviations: NIR, near-infrared; NIRS, NIR spectroscopy; μ_a, absorption coefficient; μ'_s, reduced scattering coefficient; THC, total hemoglobin concentration; StO_2, tissue blood oxygen saturation; ShO_2, hemoximeter-measured blood oxygen saturation.

†To whom correspondence should be addressed. E-mail: rgchoe@mail.sas.upenn.edu.

© 2003 by The National Academy of Sciences of the USA

www.pnas.org/cgi/doi/10.1073/pnas.1735462100

Downloaded at Palestinian Territory, occupied on December 20, 2021

www.manaraa.com

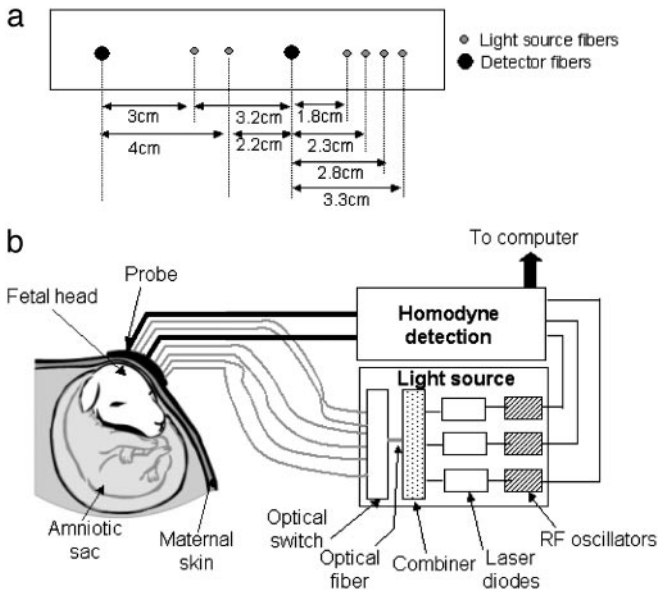

Fig. 1. Schematic of the transabdominal probe (*a*) and the NIR frequency domain instrument (*b*) to which the probe is coupled.

detail by Yu *et al.* (24). Laser diodes at 675, 786, and 830 nm are intensity modulated with three different local radio frequency oscillators operating at around 70 MHz. The light output from each laser diode is combined by using a fiber combiner into a single optical fiber. In this manner, a single optical fiber can simultaneously deliver light output from the three frequency-encoded laser diodes (24, 25). The total light output from the single optical fiber was 15 mW (3 mW at 675 nm, 9 mW at 786 nm, and 3 mW at 830 nm, respectively). An optical prism switch was used to direct the light output from the single optical fiber to the six source fiber positions on the transabdominal probe.

The detection module consists of an avalanche photodiode and two amplifiers, with a band-pass filter between them. The output from the detection module is connected to a demodulation unit, which consists of three in-phase and quadrature-phase demodulators. The in-phase and quadrature-phase signals are low-pass filtered, digitized, and then converted into diffuse wave signal amplitude and phase. Total acquisition time for the NIR photon diffusion measurements at the three wavelengths and 12 source-detector separations was 1 s.

This instrument has been extensively tested in tissue phantoms and in rat brain studies (24). The noise equivalent power is <10 pW/$\sqrt{\text{Hz}}$, and the dynamic range is >70 dB (amplitude errors $< \pm 1\%$ and phase error $< 1°$). The instrument has very low inter-channel crosstalk (<-80 dB) and good long-term stability (amplitude errors $< \pm 1\%$ and phase error $< 1°$ in 30 min).

Animal Protocol. Five pregnant ewes (132–144 days gestation) were evaluated in this study. The animals were handled according to the National Institutes of Health guidelines of the Institutional Animal Care and Use Committee. The protocol consisted of the following steps: (*i*) anesthesia and catheterization of the pregnant ewe, (*ii*) catheterization of the fetus, (*iii*) catheterization of the ewe for aortic occlusion, and (*iv*) NIR photon diffusion measurements and fetal blood sampling during baseline, hypoxia, and recovery.

First, the pregnant ewe was anesthetized with halothane (26). The carotid artery was catheterized for maternal arterial blood sampling and blood pressure monitoring. Second, the uterus was exposed by a mid-line abdominal incision, and a small hysterotomy was performed to expose the fetus for catheterization. The left brachial artery was catheterized for fetal arterial blood sampling and the right brachial artery was catheterized for fetal blood pressure monitoring. The jugular vein was catheterized for fetal venous blood sampling. The fetal body was then placed back in the uterus. The uterus was tied around the fetal neck (purse-string method) to expose the fetal head for the transabdominal NIR measurements. The exposed head was placed directly underneath the maternal skin and secured by suturing its ears to skin. The purse-string approach was used to minimize the effect of the uterus in this pilot investigation.

Then, a catheter with an inflatable balloon was inserted through the femoral artery of the pregnant ewe for aortic occlusion. Aortic occlusion through the femoral artery of the pregnant ewe is expected to directly reduce uterine blood flow to the fetus but has a minimal effect on maternal oxygenation.

Finally, the probe was placed on the maternal abdomen directly above the fetal head, as shown in Fig. 1*b*. The NIR measurements commenced and were performed continuously during the entire baseline-hypoxia-recovery cycle. Fetal arterial and venous blood samples were drawn during the baseline NIR measurement. Then the balloon was inflated to block uterine blood flow and induce fetal hypoxia. The balloon was inflated until the fetal blood pressure dropped rapidly. The inflation was maintained for 209 ± 38 s. Then the balloon was deflated and the fetus was allowed to recover. Blood samples were drawn from fetus every 30 s during hypoxia and once after recovery. Maternal arterial blood samples were sampled and checked periodically to ensure that the maternal arterial saturation was not perturbed by aortic occlusion.

The thickness of the maternal layer was measured with a caliper to be 4.0 ± 0.4 mm. The thickness of the fetal skull was obtained postmortem, and it was 5.0 ± 0.5 mm. Maternal arterial oxygen saturation, fetal arterial oxygen saturation, and fetal venous oxygen saturation were quantified from the blood samples with an OSM3 hemoximeter (Radiometer, Copenhagen).

Data Analysis. The general steps for analysis of the NIR photon diffusion measurements are as follows. The reflected photon fluence $\Phi[\mu_a(r,\lambda),\mu'_s(r,\lambda)]$ at the surface of the medium is measured. It depends on the tissue absorption coefficient (μ_a) and reduced scattering coefficient (μ'_s) and the separation between the source and detector, r, at a given wavelength λ. μ_a and μ'_s are determined by minimizing

$$\chi^2 = \sum \left| \frac{\Phi_m}{\Phi_m^b} - \frac{\Phi_c}{\Phi_c^b} \right|^2,$$

where Φ_m is the measured fluence and Φ_c is the fluence calculated by using a photon diffusion model. Φ_m^b and Φ_c^b are the measured and calculated baseline fluences, respectively, in the initial normoxic state (i.e., before the hypoxic perturbation). After μ_a is determined, concentrations of oxyhemoglobin (C_{HbO_2}) and deoxyhemoglobin (C_{Hb}) are calculated (10). Total hemoglobin concentration (THC = $C_{Hb} + C_{HbO_2}$) and tissue blood oxygen saturation [$StO_2 = (C_{HbO_2}/\text{THC}) \times 100$] are then easily determined.

The data analysis procedure used in this study consisted of three steps: (*i*) construction of Φ_m from NIR measurements, (*ii*) formulation of Φ_c from two-layer diffusion model by using *a priori* spectral and spatial information, and (*iii*) retrieval of fetal blood saturation from χ^2 minimization (see below for details).

Sliding window (4-s) averaging was used to smooth the amplitude (A_m) and phase (θ_m) data measured over the time course of the normoxia-hypoxia-recovery cycle in each study. The measured fluence $\Phi_m(r,\lambda) = A_m exp(i\theta_m)$. The baseline fluence measurement Φ_m^b was determined by averaging the first 100 data points from the amplitude- and phase-time curves during the initial normoxic state of the fetus.

Downloaded at Palestinian Territory, occupied on December 20, 2021

www.manaraa.com

Table 1. The values of fixed parameters in the data analysis

Parameters	Top layer	Bottom layer
d	8–10 mm	
$\mu_a^{bg}(\lambda)$	$0.76\ \mu_a^{H_2O} + 0.12\ \mu_a^{lipid}$	$0.76\ \mu_a^{H_2O} + 0.12\ \mu_a^{lipid}$
b	0.5	0.5
μ'^{786nm}_s	9.5 cm^{-1}	9.5 cm^{-1}
Baseline THC	80 μM	80 μM
Baseline StO_2	80%	0.43 SaO_2 + 0.57 SvO_2

A was determined by b and μ'^{786nm}_s. SaO_2, arterial blood oxygen saturation; SvO_2, venous blood oxygen saturation.

A numerical solution to the diffusion equation for a two-layer model was used to generate Φ_c. Two-layer diffusion models have been investigated by a number of researchers by using analytical (27–31) or numerical (32, 33) solutions. Here the finite difference method was used to numerically solve the diffusion equation for a three-dimensional, two-layer model of the *in utero* system. In this model, the tissues unperturbed by aortic occlusion were approximated as the top layer whose thickness is d; this layer includes the maternal skin, fetal head skin, and the fetal skull. The fetal brain was incorporated as the bottom layer. Strictly speaking, the fetal skin is also influenced by hypoxic perturbations, but, because this layer is quite thin (≈1 mm), it was considered part of the top layer.

Incorporation of *a priori* spectral information about the absorbers and scatterers in the tissue reduces the number of unknowns and the inter-parameter crosstalk between μ_a and μ'_s (34). The wavelength dependence of μ_a is determined by the concentration of tissue absorbers and their wavelength-dependent extinction coefficients. Specifically, $\mu_a(\lambda) = \varepsilon_{HbO_2}(\lambda)C_{HbO_2} + \varepsilon_{Hb}(\lambda)C_{Hb} + \mu_a^{bg}(\lambda)$ where λ is the wavelength, ε is the extinction coefficient, C is the concentration, and μ_a^{bg} is the background absorption contributed by water and lipid. μ'_s is often modeled by a Mie scattering formula in this wavelength range, i.e., $\mu'_s(\lambda) = A\lambda^{-b}$ where A and b are determined by scatterer size and density. Instead of treating μ_a and μ'_s at each wavelength as unknowns, we use the absorber concentrations and scattering parameters A and b as unknowns in the Φ_c calculation, and then analyze all wavelengths simultaneously.

Because C_{Hb} and C_{HbO_2} of fetal brain are the major parameters of interest and make the largest contribution to the signal variation, we fixed all other parameters. Table 1 shows the fixed parameters for each layer of the two-layer model. In the top layer, d was fixed based on thickness measurements of the maternal skin, fetal skin, and fetal skull postmortem. The background $\mu_a^{bg}(\lambda)$, the scattering properties A and b, the baseline THC of both layers, and the baseline StO_2 of the top layer were assumed based on values reported in the literature (35–37). The StO_2 values of the bottom layer were obtained from the hemoximeter measurements during the normoxic baseline in each cycle. Specifically, the baseline StO_2 value for the fetus (bottom layer) was determined by using a compartmental model (38) where StO_2 is made up of 43% fetal arterial oxygen saturation and 57% fetal venous oxygen saturation. Because the aortic occlusion protocol is expected to perturb fetal hemodynamics only, the top layer THC and StO_2 were assumed to be the same as the baseline throughout the cycle. Once all of the fixed parameters were defined for the calculation of Φ_c, the MATLAB function, fminsearch, using the Nelder-Mead Simplex method (iterative method) was used for χ^2 minimization to extract fetal brain C_{Hb} and C_{HbO_2}.

To test the effect of the fixed parameters on error propagation in the two-layer diffusion algorithm, each parameter was varied within a range (≈±25%) reported in the literature. An error analysis indicated the two-layer diffusion algorithm was relatively insensitive to variations in the majority of fixed parameters.

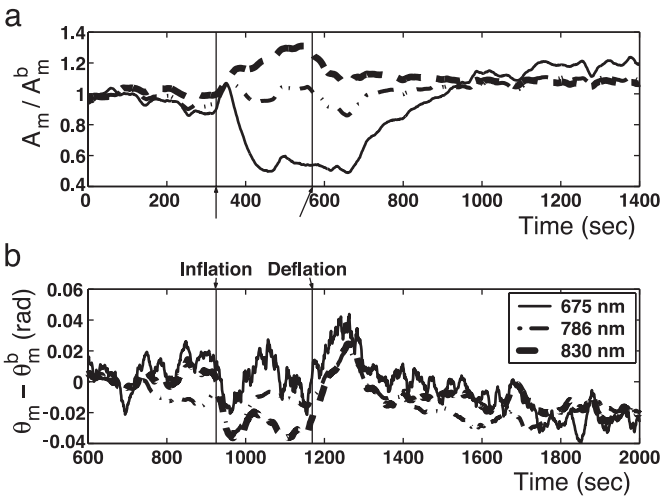

Fig. 2. Normalized measurements of amplitude (A_m/A_m^b) and the phase shift ($\theta_m - \theta_m^b$) vs. time measured at a source-detector separation of 4.0 cm during a normoxia-hypoxia-recovery cycle at wavelengths of 675, 786, and 830 nm. The amplitude and phase were normalized to the baseline amplitude and phase, which were averaged from the first 100 data points in the time trace.

Variation in these fixed parameters resulted in at most 2% variation in fetal blood saturation values. The assumptions relating arterial and venous contributions to the fetal baseline StO_2 were limiting parameters in our calculations. Varying the arterial/venous contribution from 43/57% (38) to 30/70% (39) resulted in 0.5–5% variation in calculated fetal StO_2, depending on the level of hypoxia. This variation was the basis for the fetal StO_2 error bars.

Results

Normalized measurements of amplitude (A_m/A_m^b) and phase shift ($\theta_m - \theta_m^b$) vs. time at a source-detector separation of 4.0 cm during a normoxia-hypoxia-recovery cycle are shown in Fig. 2 at wavelengths 690, 786, and 830 nm. The amplitude and phase were normalized to the baseline amplitude and phase. The effects of hypoxia are particularly evident in the amplitude vs. time trace. The decrease in amplitude at 675 nm and increase at 830 nm indicate a relative increase in the deoxy-hemoglobin concentration and a relative decrease in the oxy-hemoglobin concentration, which is the expected trend for hypoxia. The amplitude at 786 nm, which is close to the isosbestic point of hemoglobin, exhibits an intermediate response. Time traces at other source-detector separations showed similar trends, but with different magnitudes. No obvious physiological interpretation could be drawn from the phase data.

In Fig. 3, two examples of the fetal blood saturation obtained from NIR transabdominal spectroscopy and from fetal blood samples quantified with the hemoximeter are presented. There is a decrease in blood saturation with inflation and an increase in blood saturation with deflation of the balloon. The blood saturation determined from the two-layer model fit shows good agreement with the hemoximeter results. Herein, the two-layer diffusion model fits of blood saturation will be denoted as fetal tissue blood saturation (StO_2).

The correlation between fetal blood saturation measured by transabdominal NIRS and the hemoximeter was also examined. NIR blood saturations, StO_2, were selected from points in the time traces where fetal arterial and blood samples were withdrawn. Blood saturation values were calculated by using the previously described compartmental model (38, 40, 41) from the fetal arterial and venous blood saturations (measured from

Downloaded at Palestinian Territory, occupied on December 20, 2021
www.manaraa.com

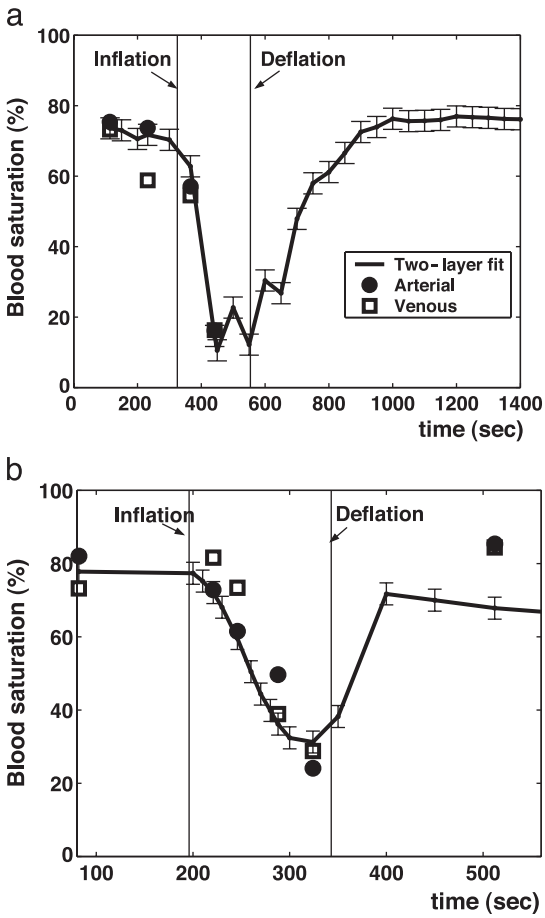

Fig. 3. Measurements in two different sheep of the fetal blood saturation obtained from NIR transabdominal spectroscopy and from fetal blood samples quantified with the hemoximeter.

the fetal blood samples by using the hemoximeter). These values served as the gold standard.

A linear relationship between the NIR and hemoximeter fetal blood saturation over a wide range of blood saturation values is observed in Fig. 4, with a correlation coefficient R equal to 0.76 ($P < 0.01$). The blood saturation data were obtained from normoxic, hypoxic, and intermediate data points ($n = 47$) collected from seven hypoxic cycles ($n = 7$). Notice the variance in blood saturation increases as the fetus progresses from a normoxic to a hypoxic state. Furthermore, there is a poorer correlation between the NIRS and hemoximeter-measured blood saturation in the lower range of blood saturations. This result may be because the blood saturation of the fetus in this range was transient so it was difficult to perfectly synchronize the NIR measurements and the blood sample withdrawals.

The baseline state (before inflation of the balloon) and stable hypoxic state (while the balloon is in the fully inflated state) was considered for further comparison. The difference between the baseline state and stable hypoxic state for the NIRS (ΔStO_2) and hemoximeter (ΔShO_2) blood saturations is compared in Fig. 5. The data are shown for two groups of hypoxia. Moderate hypoxic cycles ($n = 3$) are grouped with $\Delta StO_2 = 30 \pm 7\%$ and severe hypoxic cycles ($n = 4$) are grouped with $\Delta StO_2 = 60 \pm 5\%$. A paired t test analysis shows that ΔStO_2 and ΔShO_2 are statistically similar within the moderate and the severe group ($P < 0.05$ for null hypothesis). An unpaired t test shows that the difference between moderate and severe ΔShO_2 is significant ($P < 0.05$). This finding is true for ΔStO_2 as well.

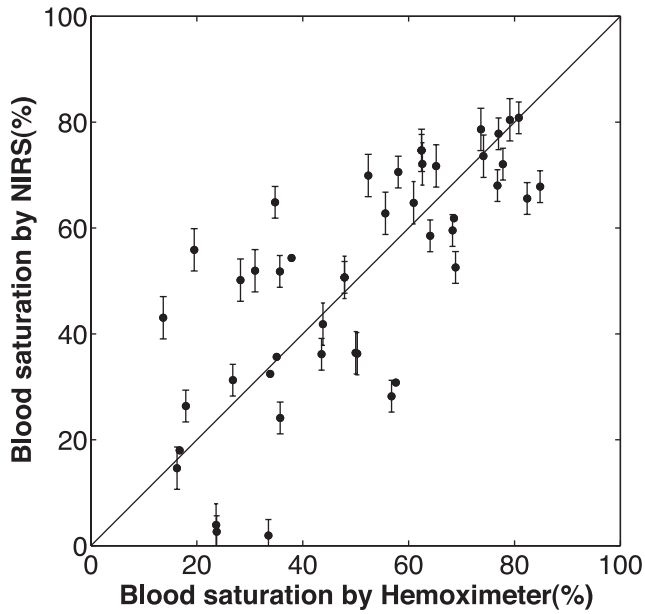

Fig. 4. Linear relationship between the fetal blood saturation measured by NIR instrument and hemoximeter over a wide range of blood saturation values with a correlation coefficient R equal to 0.76 ($P < 0.01$).

Discussion

This study demonstrates the feasibility of transabdominal NIR spectroscopy for detection and quantification of fetal hypoxia *in utero*. The pregnant ewe model is a widely used model for studies of fetal physiology and was ideally suited for this proof-of-principle study. Perturbations of fetal blood saturation were performed in a controlled manner, and fetal arterial and venous blood saturations determined from fetal blood samples served as a reliable gold standard to which the NIR-measured blood saturations could be compared. The multi-wavelength, multi-separation NIR frequency-domain instrument coupled with the numerical two-layer diffusion model proved capable of retrieving fetal blood saturation *in utero* accurately and noninvasively. The frequency-domain technique is more effective than the previous continuous-wave techniques (19,

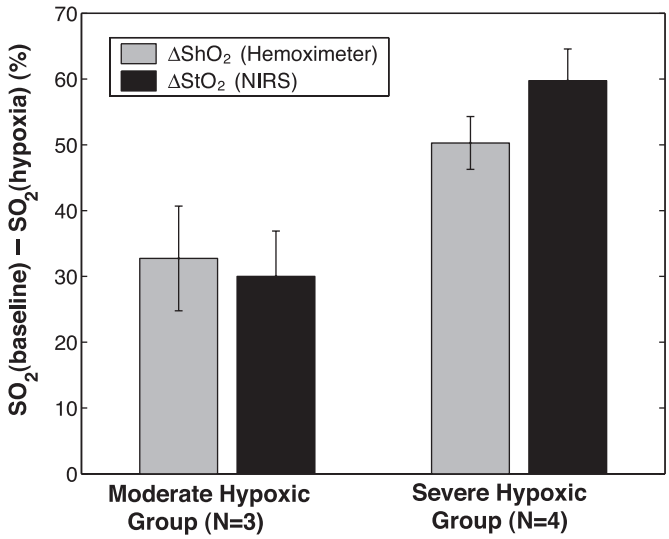

Fig. 5. Difference in blood saturation between the baseline state and stable hypoxic state for the NIRS (ΔStO_2) and hemoximeter (ΔShO_2) measured blood saturations. The data are shown for two groups of hypoxia.

MEDICAL SCIENCES

Downloaded at Palestinian Territory, occupied on December 20, 2021

www.manaraa.com

20, 22); the former is better able to decouple absorption from scattering, which is important for quantifying oxy- and deoxyhemoglobin concentrations in tissue. The two-layer numerical diffusion model also represents a significant improvement over the widely used homogeneous model; the former model was clearly able to deconvolve fetal from maternal blood saturations, rather than volume-averaging them. When the homogeneous model was used on this fetal data under the same condition, it underestimated the change in blood saturation (e.g., when $\Delta ShO_2 = 60\%$, the homogeneous model gave $\approx 5\%$). Multi-wavelength NIR photon diffusion measurements enabled the use of *a priori* spectral information to reduce the number of unknowns (absorbers) in the two-layer diffusion model. Finally, NIR reflectance measurements at multiple source-detector separations probe different tissue depths, thus optimizing the deconvolution of fetal from maternal signals using the two-layer diffusion model.

In this study, several modifications were made to the pregnant ewe model to simplify the fetal hypoxia protocol. First, hypoxia in the fetus was indirectly induced through aortic occlusion of the maternal femoral artery. Alternative approaches for inducing fetal hypoxia are to lower the maternal blood saturation by lowering the fraction of inspired oxygen (FiO_2) or through umbilical cord occlusion. These alternative approaches were evaluated in preliminary studies. The problem with lowering maternal FiO_2 was that both maternal and fetal blood saturations were affected and therefore the perturbation was not unique to the fetus. With the umbilical cord occlusion approach, fetal morbidity and mortality were significant. Another modification made in this study was that the uterine layer was removed from the field during transabdominal NIR spectroscopy of the fetus. The protocol was simplified in this manner to first establish the accuracy of quantifying fetal cerebral blood saturation, for the case in which the overlying layers are not affected by the hypoxic perturbation. The success of this pilot investigation sets the precedent for future animal model studies. In future studies, the complexity of the additional uterine layer and different perturbation approaches will be investigated. Additionally, a larger number of animals will be studied to obtain more statistically significant results.

To translate this technology to clinical settings, further improvements must be considered. Implementation of the two-layer diffusion model required information about several variables: top layer thickness, which served as *a priori* spatial information, and fetal baseline blood saturation from the hemoximeter measurements. Other parameters were assumed according to the literature values, and their variation resulted in minimal influence on the fetal blood saturation calculation. In clinical studies, the top layer thickness can be measured by ultrasound. Other available parameters, such as maternal arterial blood saturation, can be used to further constrain the variables. However, the baseline fetal blood saturation is not available in the clinical environment. If the baseline fetal blood saturation had been overestimated, the algorithm would have underestimated the severity of hypoxia in the fetus and vice versa. Absolute quantification of baseline fetal blood saturation is possible with measurements at more source-detector separations and more wavelengths (ref. 42; with extensive calibration, ref. 43). The other major difficulty arises because the distance from the maternal abdomen to the fetal brain is 2–4 cm (19) in humans. This approach, therefore, requires optimization of the instrumentation toward measuring at larger source-detector separations than used in the present animal study. These issues will be explored in future studies.

We thank A. Hielscher, P. W. Nathanielsz, Z. Liu, M. J. Holboke, and J. P. Culver for useful discussion and collaborations and Y. Choe for his illustration. This work was supported by National Institutes of Health Small Business Innovation Research Grants R43-HL61057-01 and R43-HL61057-02. A.G.Y. acknowledges partial support from National Institutes of Health Grant 2-R01-HL57835-04.

1. Vannucci, R. C. & Perlman, J. M. (1997) *Pediatrics* **100,** 1004–1014.
2. Vannucci, R. C. (2000) *Am. J. Perinatol.* **17,** 113–120.
3. Toft, P. B. (1999) *Pediatr. Neurol.* **21,** 602–610.
4. Lavery, J. (1990) *Clin. Obstet. Gynecol.* **25,** 689–705.
5. Manning, F. A., Harman, C. R. & Morrison, I. (1990) *Am. J. Obstet. Gynecol* **162,** 703–709.
6. Prentice, A. & Lind, T. (1987) *Lancet* **2,** 1375–1377.
7. Haskell, R. C., Svaasand, L. O., Tsay, T., Feng, T., McAddams, M. S. & Tromberg, B. J. (1994) *J. Opt. Soc. Am. A* **11,** 2727–2741.
8. Chance, B. (1991) *Annu. Rev. Biophys. Biophys. Chem.* **20,** 1–28.
9. Yodh, A. & Chance, B. (1995) *Phys. Today* **48,** 34–40.
10. Yodh, A. G. & Boas, D. A. (2003) *Biomedical Photonics Handbook* (CRC, Boca Raton, FL), Chap. 21.
11. Boas, D. A., Brooks, D. H., Miller, E. L., DiMarzio, C. A., Kilmer, M., Gaudette, R. J. & Zhang, Q. (2001) *IEEE Signal Proc. Mag.* **18,** 57–75.
12. Duncan, A., Meek, J. H., Clemence, M., Elwell, C. E., Fallon, P., Tyszczuk, L., Cope, M. & Delpy, D. T. (1996) *Pediatr. Res.* **39,** 889–894.
13. Chen, Y., Zhou, S. M., Xie, C. H., Nioka, S., Delivoria-Papadopoulos, M., Anday, E. & Chance, B. (2000) *J. Biomed. Opt.* **5,** 194–200.
14. Kurth, C. D., Steven, J. L., Montenegro, L. M., Watzman, H. M., Gaynor, J. W., Spray, T. L. & Nicolson, S. C. (2001) *Ann. Thorac. Surg.* **72,** 187–192.
15. Hintz, S. R., Benaron, D. A., Siegel, A. M., Zourabian, A., Stevenson, D. K. & Boas, D. A. (2001) *J. Perinat. Med.* **29,** 335–343.
16. Hebden, J. C., Gibson, A., Yusof, R. M., Everdell, N., Hillman, E. M. C., Delpy, D. T., Arridge, S. R., Austin, T., Meek, J. H. & Wyatt, J. S. (2002) *Phys. Med. Biol.* **47,** 4155–4166.
17. Dildy, C. (1996) *Am. J. Obstet. Gynecol.* **175,** 1–9.
18. Garite, T. J., Dildy, G. A., McNamara, H., Nageotte, M. P., Boehm, F. H., Dellinger, E. H., Knuppel, R. A., Porreco, R. P., Miller, H. S., Sunderji, S., Varner, M. W. & Swedlow, D. B. (2000) *Am. J. Obstet. Gynecol.* **183,** 1049–1058.
19. Ramanujam, N., Long, H., Rode, M., Forouzan, I., Morgan, M. & Chance, B. (1999) *J. Matern. Fetal Med.* **8,** 275–288.
20. Ramanujam, N., Vishnoi, G., Hielscher, A. H., Rode, M., Forouzan, I. & Chance, B. (2000) *J. Biomed. Opt.* **5,** 173–184.
21. Zourabian, A., Siegel, A., Chance, B., Ramanujam, N., Rode, M. & Boas, D. A. (2000) *J. Biomed. Opt.* **5,** 391–405.
22. Vishnoi, G., Hielscher, A. H., Ramanujam, N. & Chance, B. (2000) *J. Biomed. Opt.* **5,** 163–172.
23. Jacques, S. L., Ramanujam, N., Vishnoi, G., Choe, R. & Chance, B. (2000) *J. Biomed. Opt.* **5,** 277–282.
24. Yu, G., Durduran, T., Furuya, D., Greenberg, J. H. & Yodh, A. G. (2003) *Appl. Opt.* **42,** 2931–2939.
25. Yang, Y. S., Liu, H. L., Li, X. D. & Chance, B. (1997) *Opt. Eng.* **36,** 1562–1569.
26. Nijland, M. J. M., Shankar, U., Iyer, V. & Ross, M. G. (2000) *Am. J. Obstet. Gynecol.* **183,** 1549–1553.
27. Boas, D. A. & Yodh, A. G. (1997) *J. Opt. Soc. Am. A.* **14,** 192–215.
28. Kienle, A. & Glanzmann, T. (1999) *Phys. Med. Biol.* **44,** 2689–2702.
29. Alexandrakis, G., Farrell, T. J. & Patterson, M. S. (2000) *Appl. Opt.* **39,** 2235–2244.
30. Pham, T. H., Spott, T., Svaasand, L. O. & Tromberg, B. J. (2000) *Appl. Opt.* **39,** 4733–4745.
31. Ripoll, J., Ntziachristos, V., Culver, J. P., Pattanayak, D. N., Yodh, A. G. & Nieto-Vesperinas, M. (2001) *J. Opt. Soc. Am. A* **18,** 821–830.
32. Dehghani, H., Arridge, S. R., Schweiger, M. & Delpy, D. T. (2000) *J. Opt. Soc. Am. A* **17,** 1659–1670.
33. Zhao, H. J., Tanikawa, Y., Gao, F., Onodera, T., Sassaroli, A., Tanaka, K. & Yamada, Y. (2002) *Phys. Med. Biol.* **47,** 2075–2093.
34. Durduran, T., Choe, R., Culver, J. P., Zubkov, L., Holboke, M. J., Giammarco, J., Chance, B. & Yodh, A. G. (2002) *Phys. Med. Biol.* **47,** 2847–2861.
35. Woodard, H. Q. & White, D. R. (1986) *Br. J. Radiol.* **59,** 1209–1219.
36. Matcher, S. J., Cope, M. & Delpy, D. T. (1997) *Appl. Optics* **36,** 386–396.
37. Taroni, P., Pifferi, A., Torricelli, A., Comelli, D. & Cubeddu, R. (2003) *Photochem. Photobiol. Sci.* **2,** 124–129.
38. Culver, J. P., Durduran, T., Furuya, D., Chueung, C., Greenberg, J. H. & Yodh, A. G. (2003) *J. Cereb. Blood Flow Metab.* **23,** 911–924.
39. Henson, L. C., Calalang, C., Temp, J. A. & Ward, D. S. (1998) *Anesthesiology* **88,** 58–65.
40. Cheung, C., Culver, J. P., Yodh, A. G., Takahashi, K. & Greenberg, J. H. (2001) *Phys. Med. Biol.* **46,** 2053–2065.
41. Gesztelyu, G., Finnegan, W., DeMaro, J. A., Wang, J. Y. & Chen, J. L. (1993) *Brain Res.* **611,** 249–257.
42. Corlu, A., Durduran, T., Choe, R., Schweiger, M., Hillman, E. M. C., Arridge, S. R. & Yodh, A. G. (2003) *Opt. Lett.*, in press.
43. Boas, D. A., Gaudette, T. J. & Arridge, S. R. (2001) *Opt. Express* **8,** 263–270.

Downloaded at Palestinian Territory, occupied on December 20, 2021
www.manaraa.com